



1 Aqueous SOA formation from photosensitized guaiacol oxidation: 2 Comparison between non-phenolic and phenolic 3 methoxybenzaldehydes as photosensitizers in the absence and 4 presence of ammonium nitrate

5 Brix Raphael Go^{1,2}, Yong Jie Li³, Dan Dan Huang⁴, Yalin Wang³, and Chak K. Chan^{1,2*}

6 ¹School of Energy and Environment, City University of Hong Kong, Hong Kong, China

7 ²City University of Hong Kong Shenzhen Research Institute, Shenzhen, China

8 ³Department of Civil and Environmental Engineering, and Centre for Regional Ocean, Faculty of Science and Technology,
9 University of Macau, Macau, China

10 ⁴Shanghai Academy of Environmental Sciences, Shanghai 200233, China

11

12 *Correspondence to:* Chak K. Chan (Chak.K.Chan@cityu.edu.hk)

13 **Abstract.** Aromatic carbonyls (e.g., methoxybenzaldehydes), an important class of photosensitizers, are abundant in the
14 atmosphere. This study compared non-phenolic (3,4-dimethoxybenzaldehyde, DMB) and phenolic (vanillin, VL)
15 methoxybenzaldehydes as photosensitizers for aqueous secondary organic aerosol (aqSOA) formation via guaiacol (GUA)
16 oxidation under atmospherically relevant cloud and fog conditions. The effects of ammonium nitrate (AN) on these reactions
17 were also explored. GUA oxidation by triplet excited states of DMB (³DMB*) (GUA+DMB) was ~4 times faster and
18 exhibited greater light absorption than oxidation by ³VL* (GUA+VL). Both GUA+DMB and GUA+VL formed aqSOA
19 composed of oligomers, functionalized monomers, oxygenated ring-opening species, and N-containing products in the
20 presence of AN. The observation of N-heterocycles such as imidazoles indicates the participation of ammonium in the
21 reactions. The majority of generated aqSOA are potential brown carbon (BrC) chromophores. Oligomerization and
22 functionalization dominated in GUA+DMB and GUA+VL, but functionalization appeared to be more important in
23 GUA+VL due to contributions from VL itself. AN did not significantly affect the oxidation kinetics, but it had distinct
24 effects on the product distributions, likely due to differences in the photosensitizing abilities and structural features of DMB
25 and VL. In particular, the more extensive fragmentation in GUA+DMB than in GUA+VL likely generated more N-
26 containing products in GUA+DMB+AN. In GUA+VL+AN, the increased oligomers may be due to VL-derived phenoxy
27 radicals induced by [•]OH or [•]NO₂ from nitrate photolysis. Furthermore, increased nitrated products observed in the presence
28 of both DMB or VL and AN than in AN alone implies that photosensitized reactions may promote nitration. This work
29 demonstrates how the structural features of photosensitizers affect aqSOA formation via non-carbonyl phenol oxidation.
30 Potential interactions between photosensitization and AN photolysis were also elucidated. These findings facilitate a better



understanding of photosensitized aqSOA formation and highlight the importance of ammonium nitrate photolysis in these reactions.

1 Introduction

Photosensitized reactions involving triplet excited states of organic compounds ($^3C^*$) are efficient pathways for the formation of secondary organic aerosol in the aqueous phase (aqSOA; Smith et al., 2014, 2016; Yu et al., 2014, 2016; Chen et al., 2020; Jiang et al., 2021; Misovich et al., 2021; Mabato et al., 2022). Upon irradiation by solar radiation, photosensitizers form an excited triplet state that directly reacts with substrates (e.g., phenols), and can generate singlet oxygen (1O_2), superoxide ($O_2^{\cdot-}$) or hydroperoxyl ($^{\cdot}HO_2$) radicals, and hydroxyl radicals ($^{\cdot}OH$) upon reactions with O_2 and substrates (George et al., 2018; Chen et al., 2020), thereby facilitating the oxidation of rather volatile species and contributing to aqSOA formation. An important class of photosensitizers is aromatic carbonyls (e.g., methoxybenzaldehydes) which are abundant in aerosol particles, cloud waters, and fog waters (Anastasio et al., 1997; Felber et al., 2021). Aromatic carbonyls can be emitted from anthropogenic sources and biomass burning (BB; Lipari et al., 1984; Edye and Richards, 1991; Hawthorne et al., 1992; Simoneit et al., 1993, 1999; Anastasio et al., 1997; Felber et al., 2021), or formed via atmospheric oxidation of aromatic hydrocarbons (Hoshino et al., 1978; Calvert and Madronich, 1987; Anastasio et al., 1997; Felber et al., 2021). BB is also a significant source of phenols through lignin pyrolysis (Simpson et al., 2005). Phenolic carbonyls have a hydroxyl ($-OH$) group on the aromatic ring, whereas non-phenolic carbonyls do not. BB smoke has been reported to have comparable concentrations of phenolic and non-phenolic carbonyls (Simoneit et al., 1993; Anastasio et al., 1997).

Most previous studies on aqSOA formation via photosensitized non-carbonyl phenol oxidation have examined 3,4-dimethoxybenzaldehyde (DMB), a non-phenolic methoxybenzaldehyde, as the photosensitizer (Smith et al., 2014, 2015; Yu et al., 2014, 2016; Chen et al., 2020; Jiang et al., 2021; Misovich et al., 2021). By contrast, phenolic carbonyls have been mainly studied as aqSOA precursors via $^{\cdot}OH$ -, nitrate-, nitrite-, and $^3DMB^*$ -mediated oxidation (Li et al., 2014; Huang et al., 2018; Pang et al., 2019; Jiang et al., 2021; Misovich et al., 2021). However, strongly light-absorbing phenolic carbonyls (e.g., molar absorptivity above 300 nm $\geq 7 \times 10^3 \text{ M}^{-1} \text{ cm}^{-1}$) can also serve as photosensitizers to promote aqSOA formation (Smith et al., 2016; Mabato et al., 2022). For instance, the direct photosensitized oxidation of phenolic carbonyls (i.e., oxidation of phenolic carbonyls by their $^3C^*$ or $^3C^*$ -derived oxidants) such as vanillin (VL; another methoxybenzaldehyde) efficiently form low-volatility products, with aqSOA mass yields of up to 140% (Smith et al., 2016). Moreover, the aqSOA mass yields from the oxidation of syringol by $^3DMB^*$ and $^3VL^*$ are similar (111% and 114%, respectively; Smith et al., 2014, 2016). In addition, we recently reported that the direct photosensitized oxidation of VL and guaiacol oxidation by $^3VL^*$ yield similar products (oligomers, functionalized monomers, and oxygenated ring-opening products) as observed with $^3DMB^*$ (Yu et al., 2014; Mabato et al., 2022). Guaiacol is a non-carbonyl BB methoxyphenol with an emission rate from fireplace wood combustion in the range of 172 to 279 mg/kg (Schauer et al., 2001; Simoneit, 2002). The atmospheric



63 reactivity of methoxyphenols has recently been reviewed (Liu et al., 2022). However, our experiments were performed at a
 64 concentration (0.1 mM VL) higher than what was typically used for DMB (0.005 to 0.01 mM; Smith et al., 2014, 2015; Yu
 65 et al., 2014, 2016). Therefore, direct comparisons between photosensitization by $^3\text{DMB}^*$ and $^3\text{VL}^*$ cannot be made. Despite
 66 the above findings, much is still unknown about how aqSOA formation proceeds in systems using phenolic carbonyls as
 67 photosensitizers.

68 BB aerosols are typically internally mixed with other aerosol components, such as ammonium nitrate (AN;
 69 Zielinski et al., 2020). Hence, aromatic carbonyls and phenols may coexist with AN in BB aerosols. Nitrate and ammonium
 70 facilitate the formation of aqSOA and brown carbon (BrC) via a number of pathways. Nitrate photolysis can produce $\cdot\text{OH}$
 71 and nitrating agents (e.g., $\cdot\text{NO}_2$; Minero et al., 2007; Huang et al., 2018; Mabato et al., 2022; Wang et al., 2022; Yang et al.,
 72 2022), and ammonium reacts with carbonyls to yield N-containing heterocycles (e.g., imidazoles) and oligomers capable of
 73 UV-Vis light absorption (De Haan et al., 2009, 2011; Nozière et al., 2009, 2010, 2018; Shapiro et al., 2009; Yu et al., 2011;
 74 Lee et al., 2013; Powelson et al., 2014; Gen et al., 2018; Grace et al., 2019; Mabato et al., 2019). Furthermore, nitrate
 75 photolysis may be an important process for SO_2 oxidation and SOA formation in the particle phase (Gen et al., 2019a,
 76 2019b, 2022; Zhang et al., 2020, 2021, 2022), and it can potentially modify the morphology of atmospheric viscous particles
 77 (Liang et al., 2021). Yet, understanding of the effects of inorganic nitrate on aqSOA formation remains limited. In addition,
 78 aqSOA formation studies involving aromatic carbonyls and phenols have probed either photosensitization or nitrate-
 79 mediated photo-oxidation, but these reactions can occur simultaneously. For instance, we previously reported nitrated
 80 compounds, including a potential imidazole derivative from the direct photosensitized oxidation of VL in the presence of AN
 81 (Mabato et al., 2022). Accordingly, investigations on reaction systems including both photosensitizers and AN may provide
 82 further insights into the aqueous-phase processing of BB aerosols.

83 In this work, we compared aqSOA formation from photosensitized guaiacol (GUA) oxidation by $^3\text{C}^*$ of non-
 84 phenolic and phenolic methoxybenzaldehydes under identical conditions (simulated sunlight and concentration) relevant to
 85 cloud and fog waters. The effects of AN on photosensitized aqSOA formation were also examined. In this study, the
 86 dominant aqSOA precursor is GUA (Henry's law constant of $9.2 \times 10^2 \text{ M atm}^{-1}$; Sagebiel et al., 1992), and DMB and VL
 87 were used as photosensitizers to oxidize GUA. DMB and VL (Henry's law constants of $5.4 \times 10^1 \text{ M atm}^{-1}$ and $4.7 \times 10^5 \text{ M}$
 88 atm^{-1} , respectively; Yaws, 1994; EPI Suite version 4.1, 2012; Felber et al., 2021), which are also abundant in BB emissions
 89 (Schauer et al., 2001; Li et al., 2014; Chen et al., 2017; Pang et al., 2019; Mabato et al., 2022) and whose structures differ
 90 only by one functional group ($-\text{OCH}_3$ for the former and $-\text{OH}$ for the latter, Fig. 1), represented non-phenolic and phenolic
 91 methoxybenzaldehydes, respectively. The structures of GUA, DMB, and VL are provided in Figure 1. Based on their
 92 quantum yield of $^3\text{C}^*$ formation, DMB and VL have been classified as moderate and poor photosensitizers, respectively
 93 (Felber et al., 2021). The photosensitized oxidation of GUA by $^3\text{DMB}^*$ or $^3\text{VL}^*$ in the absence (and presence) of AN are
 94 referred to as GUA+DMB(+AN) and GUA+VL(+AN), respectively. GUA photo-oxidation by AN alone (GUA+AN) was
 95 also explored for comparison with GUA+DMB+AN and GUA+VL+AN. The molar absorptivities of GUA, DMB, VL, and



96 nitrate are shown in Figure 1. The precursor and photosensitizer decay kinetics, detected products, and absorbance
97 enhancement were used to characterize the reactions.

98 While several studies on photo-oxidation of BB emissions are available, this work focuses on the comparison
99 between non-phenolic and phenolic methoxybenzaldehydes as photosensitizers in the absence and presence of AN for
100 aqSOA formation. We found that GUA oxidation by $^3\text{DMB}^*$ was faster and exhibited greater light absorption relative to
101 GUA+VL. These are likely attributed to the stronger photosensitizing ability of DMB and the –OH group of VL, making it
102 more prone to oxidation and more reactive towards electrophilic aromatic substitution. Oligomerization and functionalization
103 dominated in GUA+DMB and GUA+VL, but functionalization appeared to be more significant in GUA+VL due to VL
104 transformation products. Although AN did not significantly influence the oxidation kinetics due to the predominant role of
105 photosensitizer chemistry compared to nitrate, AN promoted the formation of N-containing products. These include N-
106 heterocycles (e.g., imidazoles), suggesting the participation of ammonium in the reactions. Moreover, the product
107 distributions indicate distinct interactions between photosensitization by $^3\text{DMB}^*$ and $^3\text{VL}^*$ and AN photolysis. In particular,
108 AN generated more N-containing products in GUA+DMB+AN and increased the oligomers in GUA+VL+AN. Furthermore,
109 increased nitrated compounds in GUA+DMB+AN and GUA+VL+AN compared to GUA+AN suggest that photosensitized
110 reactions may promote reactions by nitrate photolysis.

111 2 Methods

112 2.1 Aqueous phase photo-oxidation experiments

113 Procedures for the photo-oxidation experiments are presented in detail in our previous study (Mabato et al., 2022).
114 Experimental solutions were prepared using 0.1 mM guaiacol (GUA, Sigma Aldrich, $\geq 98.0\%$) and 0.01 mM 3,4-
115 dimethoxybenzaldehyde (DMB, Acros Organics, 99+%) or 0.01 mM vanillin (VL, Acros Organics, 99%, pure), in the
116 absence and presence of ammonium nitrate (1 mM; AN, Acros Organics, 99+%, for analysis). These GUA and
117 methoxybenzaldehydes concentrations are within the values expected in cloud or fog drops in areas with significant wood
118 combustion (Anastasio et al., 1997; Rogge et al., 1998; Nolte et al., 2001). The AN concentration represents values usually
119 observed in cloud and fog waters (Munger et al., 1983; Collett et al., 1998; Zhang and Anastasio, 2003; Li et al., 2011;
120 Giulianelli et al., 2014; Bianco et al., 2020). It must be noted that this study did not intend to identify the AN concentrations
121 that would affect the kinetics but attempted to analyze the effects of AN on photosensitized aqSOA formation. A solution
122 composed of 0.1 mM GUA and 1 mM AN (GUA+AN) was also examined for comparison with GUA+DMB+AN and
123 GUA+VL+AN. Sulfuric acid (H_2SO_4 ; Acros Organics, ACS reagent, 95% solution in water) was used to adjust the pH of the
124 solutions to 4, which is within typical cloud pH values (2–7; Pye et al., 2020) and pH values observed in wood burning-
125 impacted cloud and fog waters (Collett et al., 1998; Raja et al., 2008). The solutions were bubbled with synthetic air for 30
126 min before irradiation and throughout the reactions to achieve air-saturated conditions (Du et al., 2011; Chen et al., 2020)
127 and were continuously magnetically stirred. In this study, the reactions can generate $^3\text{DMB}^*/^3\text{VL}^*$ and secondary oxidants



($^1\text{O}_2$, $\text{O}_2^{\cdot-}/\text{HO}_2$, $\cdot\text{OH}$) but not ozone. Solutions contained in a quartz photoreactor were irradiated using a xenon lamp (model 6258, Ozone free xenon lamp, 300 W, Newport) equipped with a longpass filter (20CGA-305 nm cut-on filter, Newport) to eliminate light below 300 nm. The reaction temperatures were maintained at 27 ± 2 °C using cooling fans positioned around the photoreactor and lamp housing. The averaged initial photon flux in the reactor measured from 300 to 380 nm was $\sim 3 \times 10^{15}$ photons $\text{cm}^{-2} \text{s}^{-1} \text{nm}^{-1}$ (Fig. 1), similar to our previous work (Mabato et al., 2022). Samples were collected every 30 mins for 180 mins for offline analyses of (1) GUA, DMB, and VL concentrations using ultra-high-performance liquid chromatography with photodiode array detector (UHPLC-PDA); (2) reaction products using UHPLC coupled with heated electrospray ionization Orbitrap mass spectrometry (UHPLC-HESI-Orbitrap-MS) operated in positive and negative ion modes; (3) concentrations of small organic acids using ion chromatography (IC); and (4) absorbance measurements using UV-Vis spectrophotometry. Each experiment was repeated independently at least three times. The reported decay rate constants, small organic acids concentration, and absorbance enhancement were averaged from triplicate experiments, and the corresponding errors represent one standard deviation. The pseudo-first-order rate constant (k') for GUA decay was determined using the following equation (Huang et al., 2018):

$$\ln ([\text{GUA}]_t / [\text{GUA}]_0) = -k't \quad (\text{Eq. 1})$$

where $[\text{GUA}]_t$ and $[\text{GUA}]_0$ are GUA concentrations at time t and 0, respectively. DMB or VL decay rate constants were calculated by replacing GUA with DMB or VL in Eq. 1. The decay rate constants were normalized to the photon flux measured for each experiment through dividing k' by the measured 2-nitrobenzaldehyde (2NB; a chemical actinometer) decay rate constant, $j(2\text{NB})$ (Mabato et al., 2022). Moreover, two independently prepared samples for each reaction condition were analyzed using UHPLC-HESI-Orbitrap-MS. Only peaks that were reproducibly detected in both sets of samples were considered. For clarity, the formulas discussed in this work correspond to neutral analytes (e.g., with H^+ or NH_4^+ removed from the ion formula). The details of the analytical procedures are provided in the Supplement (Sects. S1 to S4).

2.2 Calculation of the normalized abundance of products

The normalized abundance of products ($[\text{P}]$, unitless) was introduced in our previous work (Mabato et al., 2022). Briefly, equal ionization efficiencies of different compounds, which is commonly used to estimate O:C ratios of SOA (Bateman et al., 2012; Lin et al., 2012; Laskin et al., 2014; De Haan et al., 2019) was assumed for the calculation:

$$[\text{P}] = \frac{A_{\text{P},t}}{A_{\text{GUA},t}} \cdot \frac{[\text{GUA}]_t}{[\text{GUA}]_0} \quad (\text{Eq. 2})$$

where $A_{\text{P},t}$ and $A_{\text{GUA},t}$ are the extracted ion chromatogram (EIC) peak areas of the product P and GUA from UHPLC-HESI-Orbitrap-MS analyses at time t , respectively; $[\text{GUA}]_t$ and $[\text{GUA}]_0$ are the GUA concentrations (μM) determined using UHPLC-PDA at time t and 0, respectively. Note that the normalized abundance of products has intrinsic uncertainties due to the variability in ionization efficiencies for various compounds. Nevertheless, it is a semi-quantitative analysis that gives an



overview of how the signal intensities changed under different experimental conditions but not the quantification of the absolute product concentration.

3 Results and Discussion

Using kinetics data, MS analyses, and absorbance enhancement data, we first examined the differences between GUA+DMB and GUA+VL (Sect. 3.1). Then, we analyzed GUA+DMB+AN, GUA+VL+AN, and GUA+AN (Sect. 3.2) to explore the effects of nitrate photolysis and ammonium on photosensitized aqSOA formation.

3.1 Comparison of photosensitized GUA oxidation by non-phenolic ($^3\text{DMB}^*$) and phenolic ($^3\text{VL}^*$) methoxybenzaldehydes

Prior studies have reported that photosensitized non-carbonyl phenol oxidation in the presence of 3,4-dimethoxybenzaldehyde (DMB) and vanillin (VL) (separately) was mainly driven by $^3\text{DMB}^*$ and $^3\text{VL}^*$, respectively (Smith et al., 2014; Mabato et al., 2022), while contributions from secondary oxidants such as $^1\text{O}_2$ and $^{\bullet}\text{OH}$ were likely minor. However, both $^3\text{DMB}^*$ and $^3\text{VL}^*$ are efficiently quenched by O_2 , suggesting that energy transfer should be considered in evaluating photosensitized processes involving these methoxybenzaldehydes (Felber et al., 2021). Moreover, it was found that $^3\text{DMB}^*$, $^1\text{O}_2$, and $\text{O}_2^{\bullet-}$ were the major contributors to the photosensitized oxidation of 4-ethylguaiacol (Chen et al., 2020). Recently, the oxidation of guaiacyl acetone (a non-conjugated phenolic carbonyl) in the presence of DMB has been reported to be initiated by $^3\text{DMB}^*$, $^1\text{O}_2$, $^{\bullet}\text{OH}$, or methoxy radical ($^{\bullet}\text{OCH}_3$) (Misovich et al., 2021). Further studies are thus required to identify the specific oxidants in these reaction systems. In this study, reactions initiated in the presence of DMB or VL are collectively referred to as photosensitized reactions. The reaction conditions, initial guaiacol (GUA) and DMB or VL decay rate constants, normalized product abundance, and the chemical characteristics of aqSOA formed in this work are summarized in Table 1.

3.1.1 Kinetic analysis of photosensitization by $^3\text{DMB}^*$ and $^3\text{VL}^*$

No significant loss of GUA or photosensitizers was observed for dark experiments. Upon irradiation, the GUA decay rate constant in GUA+DMB was ~4 times higher than in GUA+VL. In GUA+DMB, the decay rate constant of GUA was ~8 times higher than that of DMB, consistent with a previous study (Smith et al., 2014). Contrastingly, the decay rate constant of VL was 2.4 times higher than that of GUA in GUA+VL. This VL consumption was also observed in our earlier work using 0.1 mM GUA + 0.1 mM VL (Mabato et al., 2022). These trends could be explained by the following reasons. First, DMB has a stronger photosensitizing ability than VL based on its higher quantum yield of $^3\text{C}^*$ formation and longer lifetime of $^3\text{DMB}^*$ compared to $^3\text{VL}^*$ (Felber et al., 2021). Second, VL is also a phenolic compound similar to GUA, and is therefore highly reactive towards oxidation. For instance, its $-\text{OH}$ group can be oxidized by $^3\text{VL}^*$ via H-atom abstraction to form phenoxy radicals which can undergo coupling to form oligomers (Kobayashi and Higashimura, 2003; Sun et al., 2010;



189 Mabato et al., 2022). The faster consumption of VL than GUA suggests a competition between ground-state VL and GUA
190 for reaction with $^3\text{VL}^*$. Moreover, compared to a $-\text{OCH}_3$ group (in DMB), an $-\text{OH}$ group (in VL) has a stronger electron-
191 donating ability and is thus more activating. Relative to DMB, VL is more reactive towards electrophilic addition of $^{\bullet}\text{OH}$ and
192 electrophilic aromatic substitution.

193 3.1.2 Product distributions and chemical characteristics of aqSOA from photosensitization by $^3\text{DMB}^*$ and $^3\text{VL}^*$

194 The products detected using UHPLC-HESI-Orbitrap-MS were used to represent the aqSOA formed in this work. The signal-
195 weighted distributions of aqSOA calculated from combined positive (POS) and negative (NEG) ion modes MS results are
196 summarized in Figure 2. The signal-weighted distributions calculated separately from POS and NEG ion modes MS results
197 are available in Figures S1 and S2. Oligomers and derivatives of GUA dominated both GUA+DMB and GUA+VL, in
198 agreement with pronounced oligomerization from triplet-mediated oxidation of relatively high phenol concentration (e.g.,
199 0.1 to 3 mM; Li et al., 2014; Yu et al., 2014, 2016; Slikboer et al., 2015; Ye et al., 2019; Mabato et al., 2022). GUA+DMB
200 had a higher oligomer contribution than GUA+VL, attributable to faster GUA oxidation by $^3\text{DMB}^*$. Figure 3 schematically
201 depicts the main differences between photosensitized GUA oxidation by $^3\text{DMB}^*$ and $^3\text{VL}^*$ in the absence and presence of
202 AN. As shown in Fig. 3, $^3\text{DMB}^*$ and $^3\text{VL}^*$ can oxidize GUA via H-atom abstraction to form phenoxy radicals which
203 undergo coupling to form oligomers (Kobayashi and Higashimura, 2003; Sun et al., 2010; Mabato et al., 2022). The higher
204 oligomer contribution in GUA+DMB is likely due to the better photosensitizing ability of DMB than VL and partly the
205 lower abundance of $^3\text{VL}^*$ due to fast VL consumption. VL was consumed faster than DMB during GUA oxidation
206 ascribable to the $-\text{OH}$ group of VL, making it more susceptible to oxidation and more reactive towards electrophilic
207 aromatic substitution. In addition, the normalized product abundance for GUA+DMB was ~ 4 times higher than that for
208 GUA+VL (Table 1), further suggesting more efficient photosensitized GUA oxidation by $^3\text{DMB}^*$ than by $^3\text{VL}^*$. The
209 oxidation of GUA or transient organic intermediates by secondary oxidants (e.g., $^1\text{O}_2$ and $^{\bullet}\text{OH}$) from $^3\text{DMB}^*$ or $^3\text{VL}^*$ and the
210 fragmentation of larger compounds generate highly oxidized ring-opening products (Yu et al., 2014; Huang et al., 2018;
211 Chen et al., 2020). GUA+DMB had a higher contribution of ring-opening products than GUA+VL, likely due to the greater
212 availability of secondary oxidants in the former and fast VL consumption lowering the production of these species in
213 GUA+VL. The IC analyses also indicate the formation of small organic acids (e.g., formic acid), which appeared to have
214 higher concentrations in the presence of DMB than in VL (Fig. S3). The reactions of secondary oxidants or ring-opening
215 products with GUA can form functionalized products. Notably, the contribution of monomers in GUA+VL was almost twice
216 as high as in GUA+DMB, ascribable to VL transformation products. We previously showed that for the direct
217 photosensitized oxidation of VL, functionalization prevails over oligomerization at 0.01 mM VL, the [VL] used in this work,
218 while oligomerization dominates at higher [VL] (0.1 mM; Mabato et al., 2022).

219 It has been reported that oligomerization could occur during the electrospray ionization process (Yasmeen et al.,
220 2010). In this work, it was confirmed that the oligomers observed were generated in the solutions via aqueous reactions



221 instead of being artefacts of HESI-MS. This is based on the absence of dimers and higher oligomers in the HESI mass
222 spectra of dark control solutions acquired by direct infusion (Yu et al., 2016).

223 The major GUA+DMB and GUA+VL products (Tables S1-S2) are mostly oligomers which can be formed through
224 the coupling of phenoxy radicals (Kobayashi and Higashimura, 2003; Sun et al., 2010; Mabato et al., 2022). GUA+DMB
225 products matched those reported in previous works on $^3\text{DMB}^*$ - and/or ^1OH -mediated phenol oxidation (Yu et al., 2014,
226 2016). These include GUA dimers and trimers (e.g., $\text{C}_{14}\text{H}_{14}\text{O}_4$ and $\text{C}_{21}\text{H}_{18}\text{O}_8$, #1 and 19; Table S1), aldehydes ($\text{C}_7\text{H}_6\text{O}_4$, #13;
227 Table S1), and esters ($\text{C}_{16}\text{H}_{18}\text{O}_6$, #14; Table S1). Functionalized products include $\text{C}_{11}\text{H}_{12}\text{O}_5$ and $\text{C}_{10}\text{H}_{12}\text{O}_3$ (#8 and 12; Table
228 S1). More than half of the major GUA+VL products are the same oligomers detected from GUA+DMB (e.g., $\text{C}_{13}\text{H}_{10}\text{O}_4$ and
229 $\text{C}_{20}\text{H}_{18}\text{O}_6$, #4 and 21; Table S1). The rest are mainly functionalized species such as $\text{C}_7\text{H}_8\text{O}_4$ and $\text{C}_8\text{H}_8\text{O}_5$ (#28 and 35; Table
230 S2), corresponding to a hydroxylated GUA and hydroxylated VL, respectively.

231 The average elemental ratios and elemental distribution of the products (Fig. S4a–d) were consistent with those in
232 previous studies on similar reaction systems (Yu et al., 2014, 2016; Mabato et al., 2022). The majority of the GUA+DMB
233 and GUA+VL products had $\text{H}:\text{C} \leq 1.0$ and $\text{O}:\text{C} \leq 0.5$, typical for aromatic species (Mazzoleni et al., 2012; Kourtchev et al.,
234 2014; Jiang et al., 2021). GUA+DMB had more compounds with higher $\text{O}:\text{C}$ (≥ 0.6), in agreement with higher contributions
235 of ring-opening products than in GUA+VL (Fig. 2). The higher $\langle \text{OS}_\text{C} \rangle$ for GUA+VL than in GUA+DMB (Table 1) was
236 probably due to the significant functionalization in the former. Moreover, the distributions of OS_C and carbon number (Fig.
237 S5a–d) show that these aqSOA products have similar elemental composition to those of low-volatility oxygenated organic
238 aerosols (LV-OOA), semi-volatile oxygenated organic aerosols (SV-OOA), and slightly with biomass burning organic
239 aerosols (BBOA) (Kroll et al., 2011). Further discussions on van Krevelen diagrams (Fig. S4a–d) and OS_C vs carbon number
240 plots (Fig. S5a–d) for GUA+DMB and GUA+VL aqSOA are available in the Supplement (Sect. S5). In brief, $^3\text{DMB}^*$ -
241 initiated GUA oxidation was faster and yielded higher normalized product abundance than oxidation by $^3\text{VL}^*$. This is likely
242 due to the stronger photosensitizing ability of DMB than VL and the $-\text{OH}$ group of VL facilitating its rapid consumption. In
243 addition, oligomerization and functionalization dominated in both GUA+DMB and GUA+VL, as reported in similar studies
244 (Yu et al., 2014, 2016; Chen et al., 2020; Jiang et al., 2021; Misovich et al., 2021; Mabato et al., 2022). However,
245 functionalization was more prominent in the latter, attributable to the transformation of VL. Nonetheless, it must be noted
246 that for phenolic aqSOA, fragmentation will ultimately be more predominant at longer irradiation times (Huang et al., 2018;
247 Yu et al., 2016; Mabato et al., 2022).

248 3.1.3 Light absorption of aqSOA from photosensitization by $^3\text{DMB}^*$ and $^3\text{VL}^*$

249 The absorbance enhancement of phenolic aqSOA generated via reactions with $^3\text{DMB}^*/^3\text{VL}^*$ has been linked to the
250 formation of conjugated structures due to oligomerization and functionalization (e.g., additions of hydroxyl and carbonyl
251 groups; Yu et al., 2014, 2016; Smith et al., 2016; Chen et al., 2020; Jiang et al., 2021; Misovich et al., 2021; Mabato et al.,
252 2022). Moreover, the aqueous-phase photo-oxidation of BB emissions can enhance BrC absorbance via the formation of
253 aromatic dimers and functionalized products (Hems et al., 2020). In this work, the absorbance enhancement of GUA+DMB



and GUA+VL (Fig. 4) correlates with oligomers and functionalized monomers, which are the highest contributors to the product signals. Identifying the chromophores responsible for the absorbance enhancement may be beneficial in understanding the impact of aqSOA on the Earth's radiative balance and determining the reactions that affect light absorption by aqSOA (Mabato et al., 2022). However, the detected products did not exhibit distinct peaks in the UHPLC-PDA chromatograms, likely due to the concentration of the chromophores being below the detection limit of PDA. Nevertheless, the higher absorbance enhancement for GUA+DMB than GUA+VL was most likely associated with the higher contribution and normalized abundance (by ~6 times) of oligomers in the former.

Additional information about aqSOA light absorption can be deduced from the plots of the double bond equivalent (DBE) values vs carbon number (n_C) (Lin et al., 2018). Figure S6 shows these plots along with the DBE reference values of fullerene-like hydrocarbons (Lobodin et al., 2012), cata-condensed polycyclic aromatic hydrocarbons (PAHs; Siegmund and Sattler, 2000), and linear conjugated polyenes with a general formula C_xH_{x+2} . The shaded area indicates a sufficient level of conjugation for visible light absorption, and species within this region are potential BrC chromophores. GUA+DMB and GUA+VL aqSOA exhibited a significant overlap in the DBE vs n_C space; nearly all products from both systems, including the high-relative-abundance species, are potential BrC chromophores. GUA+DMB had more oligomeric products with high relative abundance ($n_C \geq 12$ and $DBE \geq 8$). For GUA+VL, high-relative-abundance products also include monomeric species ($n_C = 7-8$ and 4-5 DBE) corresponding to hydroxylated products (e.g., $C_7H_8O_4$ and $C_8H_8O_5$; 28 and 35; Table S2). These observations further indicate the importance of oligomerization and functionalization for the absorbance enhancement of aqSOA generated via photosensitization by $^3DMB^*$ and $^3VL^*$. In summary, $^3DMB^*$ and $^3VL^*$ can oxidize GUA resulting in aqSOA and BrC formation, but GUA+DMB exhibited stronger light absorption. In GUA+VL, the extent of GUA oxidation was limited by significant VL consumption.

3.2 Comparison of photosensitized GUA oxidation by non-phenolic ($^3DMB^*$) and phenolic ($^3VL^*$) methoxybenzaldehydes in the presence of AN

3.2.1 Kinetic analysis of photosensitization by $^3DMB^*$ and $^3VL^*$ in the presence of AN

Ammonium nitrate (AN) did not significantly affect ($p > 0.05$) the decay rate constants of GUA, DMB, and VL for both GUA+DMB+AN and GUA+VL+AN (Table 1), likely due to the higher molar absorptivities of the photosensitizers compared to that of nitrate. This implies that the chemistry of $^3DMB^*$ and $^3VL^*$ dominated that of nitrate. In this work, the GUA decay rate constants decreased in the order of GUA+DMB/GUA+DMB+AN > GUA+VL/GUA+VL+AN > GUA+AN (Table 1). Note that as the molar absorptivities of the photosensitizers are higher than that of nitrate, the kinetics data were also analyzed on a per-photon-absorbed basis for a more appropriate comparison of reaction efficiency (Sect. S6). The apparent quantum efficiency of GUA photodegradation (ϕ_{GUA}) in the presence of nitrate (GUA+AN: $1.3 \times 10^{-2} \pm 2.9 \times 10^{-3}$) was ~2 and ~7 times higher than that in the presence of DMB ($6.6 \times 10^{-3} \pm 1.9 \times 10^{-4}$) or VL ($1.8 \times 10^{-3} \pm 4.9 \times 10^{-4}$), respectively. This suggests that nitrate-mediated GUA photo-oxidation is more efficient than photosensitization by $^3DMB^*$ or $^3VL^*$ on a per-photon-absorbed basis.



3.2.2 Product distributions and chemical characteristics of aqSOA from photosensitization by $^3\text{DMB}^*$ and $^3\text{VL}^*$ in the presence of AN

For both GUA+DMB+AN and GUA+VL+AN, AN had no significant effect on the normalized product abundance (Table 1), but it induced the formation of N-containing products composed of N-heterocycles (e.g., imidazoles and pyridines) and oligomers, as well as nitrated species. Similarly, we previously reported a potential imidazole derivative from the direct photosensitized oxidation of VL in the presence of AN, which was attributed to the reaction of ring-opening products with dissolved ammonia (Mabato et al., 2022). Oligomers remained the highest signal contributors in the presence of AN (Fig. 2), but interactions between photosensitization by $^3\text{DMB}^*$ and $^3\text{VL}^*$ and AN photolysis were distinct. First, nitrated species had similar contributions in both cases, but the contribution and normalized abundance of all N-containing products in GUA+DMB+AN were 2 and ~14 times higher, respectively, than in GUA+VL+AN. This difference can be attributed to the higher contribution of N-heterocycles and N-containing oligomers in GUA+DMB+AN. Compared to GUA+VL, GUA+DMB had a higher contribution of ring-opening products which can react with ammonia, as discussed earlier (Figs. 2 and 3). Second, the decrease in oligomers in GUA+DMB+AN may be due to their fragmentation induced by $^{\bullet}\text{OH}$ from nitrate photolysis, then conversion to N-containing products. Correspondingly, the contribution of possibly ring-retaining N-containing products in GUA+DMB+AN (18.6%) was ~3 times higher than that in GUA+VL+AN (6.5%). While fragmentation of oligomers likely occurred in GUA+VL+AN as well, the increase in oligomers suggests that other reactions have taken place. For GUA+VL+AN, $^{\bullet}\text{OH}$ or $^{\bullet}\text{NO}_2$ from nitrate photolysis may have initiated H-atom abstraction from the –OH group of VL, generating phenoxy radicals which can undergo coupling to form more oligomers (Kobayashi and Higashimura, 2003; Sun et al., 2010; Mabato et al., 2022). This may also explain the more significant decrease of monomers in GUA+VL+AN (~3 times) compared to GUA+DMB+AN (~2 times). Similarly, we previously observed an increase in oligomers upon adding 1 mM AN to 0.01 mM VL (Mabato et al., 2022), the [VL] used in this work. These findings indicate that photosensitization by non-phenolic and phenolic methoxybenzaldehydes may interact differently with AN photolysis.

GUA+AN mainly formed oligomers analogous to $^{\bullet}\text{OH}$ -mediated phenol oxidation (Yu et al., 2014, 2016), followed by N-containing products. The normalized product abundance of GUA+AN was the lowest among all experiments, likely due to the lower GUA decay constant relative to photosensitized oxidation. Moreover, the normalized abundance of N-containing products in GUA+AN was ~12 times lower than that in GUA+DMB+AN but comparable to that in GUA+VL+AN. This discrepancy for GUA+VL+AN might be due to the weaker signals of its N-containing products in the positive compared to the negative ion mode. As previously mentioned, the normalized product abundance was calculated using only the positive ion mode data as the GUA signal from the negative ion mode was weak and thus may present large uncertainties during normalization. Interestingly, the contributions from nitrated species in GUA+DMB+AN and GUA+VL+AN were higher than in GUA+AN, suggesting possible enhancement of nitration reactions. This is likely due to the increased formation of $^{\bullet}\text{NO}_2$, for instance, via the reactions of $^{\bullet}\text{OH}$ and $\text{O}_2^{\bullet-}$ (from $^3\text{DMB}^*$ or $^3\text{VL}^*$) with NO_2^- (Pang et al., 2019; Mabato et al., 2022). This implies that photosensitized reactions may promote reactions induced by nitrate photolysis.



321 The major products from GUA+DMB+AN, GUA+VL+AN, and GUA+AN (Tables S3–S5) include oligomers and
 322 functionalized monomers detected in GUA+DMB and GUA+VL (Tables S1–S2). The N-heterocycles from
 323 GUA+DMB+AN include $C_6H_6N_4$ (#41; Table S3), which may be 2,2'-biimidazole (BI), a reaction product from glyoxal +
 324 reduced nitrogenous compounds (e.g., ammonium salts) (De Haan et al., 2009; Galloway et al., 2009; Nozière et al., 2009;
 325 Shapiro et al., 2009; Yu et al., 2011; Kampf et al., 2012; Gen et al., 2018; Mabato et al., 2019). The nitrated products include
 326 $C_{12}H_{11}N_3O_3$ and $C_{15}H_{10}N_4O_3$ (#42 and 49; Table S3), which possibly have a nitrated imidazole moiety and a nitrophenol
 327 moiety, respectively. For GUA+VL+AN, oligomers ($C_{14}H_{12}O_6$ and $C_{20}H_{16}O_7$; #55 and 59, Table S4) which were not among
 328 the major products in GUA+VL were noted. $C_{10}H_8O_2$ has a furanone group (#50; Table S4); furanones are the primary
 329 products of the reaction of $\cdot OH$ with toluene and other aromatic hydrocarbons (Smith et al., 1999). Moreover, $C_{11}H_9N_3O_3$
 330 (#57; Table S4) has a nitrated imidazole moiety. Among the N-containing compounds in GUA+AN is $C_4H_3N_3O_3$ (#69; Table
 331 S5), which may be a nitrated imidazole-2-carboxaldehyde. Imidazole-2-carboxaldehyde is also a reaction product from
 332 glyoxal + reduced nitrogenous compounds (e.g., ammonium salts) (De Haan et al., 2009; Galloway et al., 2009; Nozière et
 333 al., 2009; Shapiro et al., 2009; Yu et al., 2011; Kampf et al., 2012; Gen et al., 2018; Mabato et al., 2019).

334 The $\langle O:C \rangle$ for GUA+DMB+AN and GUA+VL+AN were lower than those in the absence of AN (Table 1), likely
 335 due to the rapid formation of highly oxidized species followed by their decomposition (Huang et al., 2018). The $\langle O:C \rangle$ and
 336 $\langle H:C \rangle$ were comparable in GUA+DMB+AN and GUA+VL+AN, but the $\langle N:C \rangle$ for the former was higher, implying a greater
 337 extent of reactions involving AN. Relative to GUA+DMB+AN and GUA+VL+AN, GUA+AN had a higher $\langle N:C \rangle$, as can be
 338 expected given that AN was the only oxidant source. The lower $\langle OS_C \rangle$ of GUA+DMB+AN and GUA+VL+AN compared to
 339 GUA+AN may be attributed to triplet-initiated oxidation generating higher-molecular-weight products with less
 340 fragmentation compared to $\cdot OH$ -mediated oxidation (Yu et al., 2014; Chen et al., 2020). Nonetheless, AN generally
 341 increased the $\langle OS_C \rangle$ for both GUA+DMB and GUA+VL, with a more noticeable increase for the former, suggesting more
 342 oxidized products. Furthermore, GUA+DMB+AN and GUA+VL+AN aqSOA had mainly similar features in the OS_C vs n_C
 343 plots as those observed in the absence of AN (Fig. S5). More information on van Krevelen diagrams (Figs. S4e–h and S7)
 344 and OS_C vs n_C plots (Figs. S5e–h and S8) for GUA+DMB+AN, GUA+VL+AN, and GUA+AN aqSOA are provided in the
 345 Supplement (Sect. S7). In essence, AN had no significant effect on the decay kinetics ascribable to photosensitizer chemistry
 346 prevailing over nitrate, but it induced the formation of N-containing products. Moreover, AN modified the product
 347 distributions, albeit in different ways (Figs. 2 and 3). In particular, N-containing products were more abundant in
 348 GUA+DMB+AN, probably due to more extensive fragmentation in GUA+DMB than in GUA+VL. In GUA+VL+AN, AN
 349 promoted oligomer formation likely via the $-OH$ group of VL. Furthermore, GUA+DMB+AN and GUA+VL+AN had more
 350 nitrated products than GUA+AN, suggesting that photosensitized reactions may promote nitrate photolysis-initiated
 351 reactions.



3.2.3 Light absorption of aqSOA from photosensitization by $^3\text{DMB}^*$ and $^3\text{VL}^*$ in the presence of AN

The presence of AN also did not appreciably affect the absorbance enhancement for both GUA+DMB+AN and GUA+VL+AN (Fig. 4). For GUA+DMB+AN, the N-containing products may have offset the decrease in oligomers to maintain the absorbance enhancement observed from GUA+DMB. Wang et al. (2022) reported that nitration might contribute significantly to absorbance enhancement for methoxyphenols in sodium nitrate (Wang et al., 2022). In GUA+VL+AN, the decrease in monomers may have counteracted the increased oligomers and generated N-containing products. Compared to GUA+DMB+AN, the N-containing products from GUA+VL+AN probably had less impact on the absorbance enhancement based on their smaller signal contribution.

Similar to experiments without AN, CHO species from GUA+DMB+AN and GUA+VL+AN were mainly overlapped in the DBE vs n_C space (Fig. S6c,d) and were mostly potential BrC chromophores. In both systems, GUA dimers were the products with the highest relative abundance. For GUA+DMB+AN, products with high relative abundance also include a CHN species, while two CHON species had high n_C (18,20) and DBE (16,14) values. In GUA+VL+AN, products with high relative abundance include a CHON species ($n_C = 11$ and 9 DBE). Approximately 30% and 43% of the N-containing products for GUA+DMB+AN and GUA+VL+AN, respectively, were among the potential BrC chromophores. This suggests the possible significance of N-containing products for light absorption of aqSOA from photosensitization by methoxybenzaldehydes and AN photolysis. Correspondingly, nitroaromatic compounds and N-heterocycles are frequently noted in BBOA (Iinuma et al., 2010; Kitanovski et al., 2012; Kourtchev et al., 2016) and have been proposed to be potential contributors to BrC light absorption (Laskin et al., 2015). Relative to GUA+DMB+AN and GUA+VL+AN, only 19% of the N-containing products in GUA+AN were potential BrC chromophores (Fig. S6e,f), and these did not include CHN species. These indicate that the N-containing products formed in the presence of both photosensitizers and AN may be more significant contributors to the light absorption of phenolic aqSOA than those formed in AN only.

4 Conclusions and atmospheric implications

The photosensitized oxidation of guaiacol (GUA) by triplet excited states of 3,4-dimethoxybenzaldehyde ($^3\text{DMB}^*$) and vanillin ($^3\text{VL}^*$) (separately) in the absence and presence of ammonium nitrate (AN) were compared under identical conditions (simulated sunlight and concentration) relevant to atmospheric cloud and fog waters. Compared to GUA+VL, faster GUA oxidation and stronger light absorption were observed in GUA+DMB. Moreover, VL was consumed faster relative to DMB, limiting the extent of GUA oxidation in GUA+VL. These differences are rooted in DMB having a better photosensitizing ability than VL and the $-\text{OH}$ group of VL, making it more susceptible to oxidation and more reactive towards electrophilic aromatic substitution. Both GUA+DMB and GUA+VL generated aqSOA, including potential BrC chromophores composed of oligomers, functionalized monomers, oxygenated ring-opening products, and N-containing products in the presence of AN. The major aqSOA formation processes for GUA+DMB and GUA+VL were oligomerization and functionalization, but functionalization appeared to be more significant in GUA+VL due to VL transformation products.



AN did not significantly affect the decay kinetics due to the predominant effect of $^3\text{DMB}^*$ and $^3\text{VL}^*$ chemistry compared to nitrate, but it promoted the formation of N-containing products; these are composed of N-heterocycles (e.g., imidazoles) and oligomers and nitrated species. The observation of N-heterocycles agrees with our previous findings that ammonium participates in photosensitized oxidation of phenolic compounds in the presence of AN (Mabato et al., 2022). These results also suggest that photosensitized oxidation of phenolic compounds in the presence of AN might be an important source of N-heterocycles and nitrated products. Identifying the sources of N-heterocycles and nitrated compounds is important due to their environmental and health impacts (Laskin et al., 2009). Moreover, photosensitized reactions by non-phenolic and phenolic methoxybenzaldehydes may be differently influenced by AN photolysis. For instance, the more extensive fragmentation in GUA+DMB than in GUA+VL possibly resulted in more N-containing products in GUA+DMB+AN. Furthermore, the increased oligomers in GUA+VL+AN may be due to VL-derived phenoxy radicals induced by $\cdot\text{OH}$ or $\cdot\text{NO}_2$ from nitrate photolysis. In addition, more nitrated compounds observed in GUA+DMB+AN and GUA+VL+AN than in GUA+AN imply that photosensitized reactions may promote nitrate-mediated photolytic reactions. On a related note, the significance of photosensitization by BrC (via formation of solvated electrons; Wang et al., 2021) and marine dissolved organic matter (via $\text{O}_2^{\cdot-}$ formation; Garcia et al., 2021) in enhanced nitrite production from nitrate photolysis have been reported. A recent study from our group has shown that glyoxal photo-oxidation mediated by both nitrate photolysis and photosensitization can significantly enhance the atmospheric sink of glyoxal (Zhang et al., 2022). Further studies are needed to improve our understanding of the interplay between photosensitized reactions and nitrate photolysis.

This study demonstrates that the structural features of photosensitizers affect aqSOA formation via non-carbonyl phenol oxidation. The VL results are broadly relevant to other phenolic carbonyls, but the effects of different functional groups should still be considered. For instance, the aldehyde/ketone pair of syringaldehyde and acetosyringone, both phenolic carbonyls, have been reported to have equal reactivity towards direct photosensitized oxidation. This is due to the greater light absorption by the aldehyde form but higher quantum efficiency for loss for the ketone form (Smith et al. 2016). However, more aqSOA was observed from syringaldehyde than acetosyringone (in either AN or ammonium sulfate; Huang et al., 2018). Our findings also imply that while the contributions of photosensitization by $^3\text{VL}^*$ (and other phenolic carbonyls) to aqSOA formation would be relatively less compared to that of $^3\text{DMB}^*$ (and other non-phenolic carbonyls), these are not negligible. As both non-phenolic and phenolic carbonyls such as the methoxybenzaldehydes examined in this work are emitted in large amounts from biomass burning, future experiments should probe the aqSOA contribution of a wider variety of photosensitizers. Moreover, further experiments on photosensitized reactions in authentic particulate matter (PM) samples should be conducted in the future. Multicomponent reactions such as GUA+DMB+AN and GUA+VL+AN should also be explored for a more accurate simulation of ambient conditions. These would be useful in assessing the overall impact of photosensitized reactions and AN photolysis on aqSOA formation in areas impacted by biomass burning and high AN concentrations, and for their better representation in aqSOA models.

417



418 *Data availability.*

419 The data used in this publication are available to the community and can be accessed by request to the corresponding author.

420 *Author contributions.*

421 BRG designed and conducted the experiments; BRG and CKC wrote the paper. All co-authors contributed to the
422 discussion of the manuscript.

423 *Competing interests.*

424 The authors declare that they have no conflict of interest.

425 *Acknowledgments.*

426 C.K.C. gratefully acknowledges support from the National Natural Science Foundation of China (42075100 and 41875142)
427 and Hong Kong Research Grants Council (11304121). Y.J.L. acknowledges funding support from the Science and
428 Technology Development Fund, Macau SAR (File No. 0019/2020/A1), and a multiyear research grant (No. MYRG2018-
429 00006-FST) from the University of Macau. The authors also thank the University Research Facility in Chemical and
430 Environmental Analysis (UCEA) at The Hong Kong Polytechnic University for the use of its UHPLC-HESI-Orbitrap Mass
431 Spectrometer and Dr Sirius Tse and Dr Chi Hang Chow for assistance with sample analyses.

432 **References**

- 433 Anastasio, C., Faust, B. C., and Rao, C. J.: Aromatic carbonyl compounds as aqueous-phase photochemical sources of
434 hydrogen peroxide in acidic sulfate aerosols, fogs, and clouds. 1. Non-phenolic methoxybenzaldehydes and
435 methoxyacetophenones with reductants (phenols), *Environ. Sci. Technol.*, 31, 218–232, <https://doi.org/10.1021/es960359g>,
436 1997.
- 437
- 438 Bateman, A. P., Laskin, J., Laskin, A., and Nizkorodov, S. A.: Applications of high-resolution electrospray ionization mass
439 spectrometry to measurements of average oxygen to carbon ratios in secondary organic aerosols, *Environ. Sci. Technol.*, 46,
440 8315–832, <https://doi.org/10.1021/es3017254>, 2012.
- 441
- 442 Bianco, A., Passananti, M., Brigante, M., and Mailhot, G.: Photochemistry of the cloud aqueous phase: a review, *Molecules*,
443 25, 423, <https://doi.org/10.3390/molecules25020423>, 2020.
- 444
- 445 Calvert, J. G. and Madronich, S.: Theoretical study of the initial products of the atmospheric oxidation of hydrocarbons, *J.*
446 *Geophys. Res.*, 92, 2211–2220, <https://doi.org/10.1029/JD092iD02p02211>, 1987.
- 447
- 448 Chen, Y., Li, N., Li, X., Tao, Y., Luo, S., Zhao, Z., Ma, S., Huang, H., Chen, Y., Ye, Z., and Ge, X.: Secondary organic
449 aerosol formation from $^3\text{C}^*$ -initiated oxidation of 4-ethylguaiaicol in atmospheric aqueous-phase, *Sci. Total Environ.*, 723,
450 137953, <https://doi.org/10.1016/j.scitotenv.2020.137953>, 2020.
- 451
- 452 Chen, Z. and Anastasio, C.: Concentrations of a triplet excited state are enhanced in illuminated ice, *Environ. Sci.: Processes*
453 *Impacts*, 19, 12–21, <https://doi.org/10.1039/C6EM00534A>, 2017.
- 454
- 455 Collett, J. L. Jr., Hoag, K. J., Sherman, D. E., Bator, A., and Richards, L. W.: Spatial and temporal variations in San Joaquin
456 Valley fog chemistry, *Atmos. Environ.*, 33, 129–140, [https://doi.org/10.1016/S1352-2310\(98\)00136-8](https://doi.org/10.1016/S1352-2310(98)00136-8), 1998.
- 457



- De Haan, D. O., Hawkins, L. N., Kononenko, J. A., Turley, J. J., Corrigan, A. L., Tolbert, M. A., and Jimenez, J. L.: Formation of nitrogen-containing oligomers by methylglyoxal and amines in simulated evaporating cloud droplets, *Environ. Sci. Technol.*, 45, 984–991, <https://doi.org/10.1021/es102933x>, 2011.
- De Haan, D. O., Pajunoja, A., Hawkins, L. N., Welsh, H. G., Jimenez, N. G., De Loera, A., Zauscher, M., Andretta, A. D., Joyce, B. W., De Haan, A. C., Riva, M., Cui, T., Surratt, J. D., Cazaunau, M., Formenti, P., Gratien, A., Pangui, E., and Doussin, J-F.: Methylamine's effects on methylglyoxal-containing aerosol: chemical, physical, and optical changes, *ACS Earth Space Chem.*, 3, 1706–1716, <https://doi.org/10.1021/acsearthspacechem.9b00103>, 2019.
- De Haan, D. O., Tolbert, M. A., and Jimenez, J. L.: Atmospheric condensed-phase reactions of glyoxal with methylamine, *Geophys. Res. Lett.*, 36, No. L11819, <https://doi.org/10.1029/2009GL037441>, 2009.
- Du, Y., Fu, Q. S., Li, Y., and Su, Y.: Photodecomposition of 4-chlorophenol by reactive oxygen species in UV/air system, *J. Hazard. Mater.*, 186, 491–496, <https://doi.org/10.1016/j.jhazmat.2010.11.023>, 2011.
- Edye, L. A. and Richards, G. N.: Analysis of condensates from wood smoke. components derived from polysaccharides and lignins, *Environ. Sci. Technol.*, 25, 1133–1137, <https://doi.org/10.1021/es00018a018>, 1991.
- Felber, T., Schaefer, T., He, L., and Herrmann, H.: Aromatic carbonyl and nitro compounds as photosensitizers and their photophysical properties in the tropospheric aqueous phase, *J. Phys. Chem. A*, 125, 5078–5095, <https://doi.org/10.1021/acs.jpca.1c03503>, 2021.
- Galloway, M. M., Chhabra, P. S., Chan, A. W. H., Surratt, J. D., Flagan, R. C., Seinfeld, J. H., and Keutsch, F. N.: Glyoxal uptake on ammonium sulphate seed aerosol: reaction products and reversibility of uptake under dark and irradiated conditions, *Atmos. Chem. Phys.*, 9, 3331–3345, <https://doi.org/10.5194/acp-9-3331-2009>, 2009.
- Garcia, S. L. M., Pandit, S., Navea, J. G., and Grassian, V. H.: Nitrous acid (HONO) formation from the irradiation of aqueous nitrate solutions in the presence of marine chromophoric dissolved organic matter: comparison to other organic photosensitizers, *ACS Earth Space Chem.*, 5, 3056–3064, <https://doi.org/10.1021/acsearthspacechem.1c00292>, 2021.
- Gen, M., Huang, D. D., and Chan, C. K.: Reactive uptake of glyoxal by ammonium-containing salt particles as a function of relative humidity, *Environ. Sci. Technol.*, 52, 6903–6911, <https://doi.org/10.1021/acs.est.8b00606>, 2018.
- Gen, M., Zhang, R., Huang, D. D., Li, Y. J., and Chan, C. K.: Heterogeneous SO₂ oxidation in sulfate formation by photolysis of particulate nitrate, *Environ. Sci. Technol. Lett.*, 6, 86–91, <https://doi.org/10.1021/acs.estlett.8b00681>, 2019a.
- Gen, M., Zhang, R., Huang, D. D., Li, Y. J., and Chan, C. K.: Heterogeneous oxidation of SO₂ in sulfate production during nitrate photolysis at 300 nm: effect of pH, relative humidity, irradiation intensity, and the presence of organic compounds, *Environ. Sci. Technol.*, 53, 8757–8766, <https://doi.org/10.1021/acs.est.9b01623>, 2019b.
- Gen, M., Liang, Z., Zhang, R., Mabato, B. R. G., and Chan, C. K.: Particulate nitrate photolysis in the atmosphere, *Environ. Sci.: Atmos.*, 2, 111–127, <https://doi.org/10.1039/d1ea00087j>, 2022.
- George, C., Brüggemann, M., Hayeck, N., Tinel, L., and Donaldson, J.: Interfacial photochemistry: physical chemistry of gas-liquid interfaces, in: *Developments in Physical & Theoretical Chemistry*, edited by: Faust, J. A. and House, J. E., Elsevier, 435–457, <https://doi.org/10.1016/B978-0-12-813641-6.00014-5>, 2018.
- Giulianelli, L., Gilardoni, S., Tarozzi, L., Rinaldi, M., Decesari, S., Carbone, C., Facchini, M. C., and Fuzzi, S.: Fog occurrence and chemical composition in the Po valley over the last twenty years, *Atmos. Environ.*, 98, 394–401, <https://doi.org/10.1016/j.atmosenv.2014.08.080>, 2014.



- Grace, D. N., Sharp, J. R., Holappa, R. E., Lugos, E. N., Sebold, M. B., Griffith, D. R., Hendrickson, H. P., and, Galloway, M. M.: Heterocyclic product formation in aqueous brown carbon systems, *ACS Earth Space Chem.*, 3, 2472–2481, <https://doi.org/10.1021/acsearthspacechem.9b00235>, 2019.
- Hawthorne, S. B., Miller, D. J., Langenfeld, J. J., and Krieger, M. S.: PM-10 High-volume collection and quantitation of semi- and nonvolatile phenols, methoxylated phenols, alkanes, and polycyclic aromatic hydrocarbons from winter urban air and their relationship to wood smoke emissions, *Environ. Sci. Technol.*, 26, 2251–2262, <https://doi.org/10.1021/es00035a026>, 1992.
- Hems, R. F., Schnitzler, E. G., Bastawrous, M., Soong, R., Simpson, A. J., and Abbatt, J. P. D.: Aqueous photoreactions of wood smoke brown carbon, *ACS Earth Space Chem.*, 4, 1149–1160, <https://doi.org/10.1021/acsearthspacechem.0c0011>, 2020.
- Hoshino, M., Akimoto, H., and Okuda, M.: Photochemical oxidation of benzene, toluene, and ethylbenzene initiated by OH radicals in the gas phase, *Bull. Chem. Soc. Jpn.*, 51, 718–724, <https://doi.org/10.1246/bcsj.51.718>, 1978.
- Huang, D. D., Zhang, Q., Cheung, H. H. Y., Yu, L., Zhou, S., Anastasio, C., Smith, J. D., and Chan, C. K.: Formation and evolution of aqSOA from aqueous-phase reactions of phenolic carbonyls: comparison between ammonium sulfate and ammonium nitrate solutions, *Environ. Sci. Technol.*, 52, 9215–9224, <https://doi.org/10.1021/acs.est.8b03441>, 2018.
- Iinuma, Y., Böge, O., Gräfe, R., and Herrmann, H.: Methyl-nitrocatechols: atmospheric tracer compounds for biomass burning secondary organic aerosols, *Environ. Sci. Technol.*, 44, 8453–8459, <https://doi.org/10.1021/es102938a>, 2010.
- Jiang, W., Misovich, M. V., Hettiyadura, A. P. S., Laskin, A., McFall, A. S., Anastasio, C., and Zhang, Q.: Photosensitized reactions of a phenolic carbonyl from wood combustion in the aqueous phase—chemical evolution and light absorption properties of aqSOA, *Environ. Sci. Technol.*, 55, 5199–5211, <https://doi.org/10.1021/acs.est.0c07581>, 2021.
- Kampf, C. J., Jakob, R., and Hoffmann, T.: Identification and characterization of aging products in the glyoxal/ammonium sulfate system – implications for light-absorbing material in atmospheric aerosols, *Atmos. Chem. Phys.*, 12, 6323–6333, <https://doi.org/10.5194/acp-12-6323-2012>, 2012.
- Kitanovski, Z., Grgić, I., Vermeulen, R., Claeys, M., and Maenhaut, W.: Liquid chromatography tandem mass spectrometry method for characterization of monoaromatic nitro-compounds in atmospheric particulate matter, *J. Chromatogr. A*, 1268, 35–43, <https://doi.org/10.1016/j.chroma.2012.10.021>, 2012.
- Kobayashi, S. and Higashimura, H.: Oxidative polymerization of phenols revisited, *Prog. Polym. Sci.*, 28, 1015–1048, [https://doi.org/10.1016/S0079-6700\(03\)00014-5](https://doi.org/10.1016/S0079-6700(03)00014-5), 2003.
- Kourtchev, I., Fuller, S. J., Giorio, C., Healy, R. M., Wilson, E., O'Connor, I., Wenger, J. C., McLeod, M., Aalto, J., Ruuskanen, T. M., Maenhaut, W., Jones, R., Venables, D. S., Sodeau, J. R., Kulmala, M., and Kalberer, M.: Molecular composition of biogenic secondary organic aerosols using ultrahigh-resolution mass spectrometry: comparing laboratory and field studies, *Atmos. Chem. Phys.*, 14, 2155–2167, <https://doi.org/10.5194/acp-14-2155-2014>, 2014.
- Kourtchev, I., Godoi, R. H. M., Connors, S., Levine, J. G., Archibald, A. T., Godoi, A. F. L., Paralovo, S. L., Barbosa, C. G. G., Souza, R. A. F., Manzi, A. O., Seco, R., Sjostedt, S., Park, J., Guenther, A., Kim, S., Smith, J., Martin, S. T., and Kalberer, M.: Molecular composition of organic aerosols in central Amazonia: an ultra-high-resolution mass spectrometry study, *Atmos. Chem. Phys.*, 16, 11899–11913, <https://doi.org/10.5194/acp-16-11899-2016>, 2016.
- Kroll, J. H., Donahue, N. M., Jimenez, J. L., Kessler, S. H., Canagaratna, M. R., Wilson, K. R., Altieri, K. E., Mazzoleni, L. R., Wozniak, A. S., Bluhm, H., Mysak, E. R., Smith, J. D., Kolb, C. E., and Worsnop, D. R.: Carbon oxidation state as a



- metric for describing the chemistry of atmospheric organic aerosol, *Nat. Chem.*, 3, 133–139, <https://doi.org/10.1038/nchem.948>, 2011.
- Laskin, A., Smith, J. S., and Laskin, J.: Molecular characterization of nitrogen-containing organic compounds in biomass burning aerosols using high-resolution mass spectrometry, *Environ. Sci. Technol.*, 43, 3764–3771, <https://doi.org/10.1021/es803456n>, 2009.
- Laskin, A., Laskin, J., and Nizkorodov, S. A.: Chemistry of atmospheric brown carbon, *Chem. Rev.*, 115, 4335–4382, <https://doi.org/10.1021/cr5006167>, 2015.
- Laskin, J., Laskin, A., Nizkorodov, S. A., Roach, P., Eckert, P., Gilles, M. K., Wang, B., Lee, H. J., and Hu, Q.: Molecular selectivity of brown carbon chromophores, *Environ. Sci. Technol.*, 48, 12047–12055, <https://doi.org/10.1021/es503432r>, 2014.
- Lee, A. K. Y., Zhao, R., Li, R., Liggio, J., Li, S., and Abbatt, J. P. D.: Formation of light absorbing organo-nitrogen species from evaporation of droplets containing glyoxal and ammonium sulfate, *Environ. Sci. Technol.*, 47, 12819–12826, <https://doi.org/10.1021/es402687w>, 2013.
- Li, P., Li, X., Yang, C., Wang, X., Chen, J., and Collett, J. L. Jr.: Fog water chemistry in Shanghai, *Atmos. Environ.*, 45, 4034–4041, <https://doi.org/10.1016/j.atmosenv.2011.04.036>, 2011.
- Li, Y. J., Huang, D. D., Cheung, H. Y., Lee, A. K. Y., and Chan, C. K.: Aqueous-phase photochemical oxidation and direct photolysis of vanillin - a model compound of methoxy phenols from biomass burning, *Atmos. Chem. Phys.*, 14, 2871–2885, <https://doi.org/10.5194/acp-14-2871-2014>, 2014.
- Liang, Z., Zhang, R., Gen, M., Chu, Y., and Chan, C. K.: Nitrate photolysis in mixed sucrose–nitrate–sulfate particles at different relative humidities, *J. Phys. Chem. A*, 125, 3739–3747, <https://doi.org/10.1021/acs.jpca.1c00669>, 2021.
- Lin, P., Yu, J. Z., Engling, G., and Kalberer, M.: Organosulfates in humic-like substance fraction isolated from aerosols at seven locations in East Asia: a study by ultra-high-resolution mass spectrometry, *Environ. Sci. Technol.*, 46, 13118–13127, <https://doi.org/10.1021/es303570v>, 2012.
- Lin, P., Fleming, L. T., Nizkorodov, S. A., Laskin, J., and Laskin, A.: Comprehensive molecular characterization of atmospheric brown carbon by high resolution mass spectrometry with electrospray and atmospheric pressure photoionization, *Anal. Chem.*, 90, 12493–12502, <https://doi.org/10.1021/acs.analchem.8b02177>, 2018.
- Lipari, F., Dasch, J. M., and Scruggs, W. F.: Aldehyde emissions from wood-burning fireplaces, *Environ. Sci. Technol.*, 18, 326–330, <https://doi.org/10.1021/es00123a007>, 1984.
- Liu, C., Chen, D., and Chen, X.: Atmospheric reactivity of methoxyphenols: a review, *Environ. Sci. Technol.*, 56, 2897–2916, <https://doi.org/10.1021/acs.est.1c06535>, 2022.
- Lobodin, V. V., Marshall, A. G., and Hsu, C. S.: Compositional space boundaries for organic compounds, *Anal. Chem.*, 84, 3410–3416, <https://doi.org/10.1021/ac300244f>, 2012.
- Mabato, B. R. G., Gen, M., Chu, Y., and Chan, C. K.: Reactive uptake of glyoxal by methylammonium-containing salts as a function of relative humidity, *ACS Earth Space Chem.*, 3, 150–157, <https://doi.org/10.1021/acsearthspacechem.8b00154>, 2019.



- Mabato, B. R. G., Lyu, Y., Ji, Y., Li, Y. J., Huang, D. D., Li, X., Nah, T., Lam, C. H., and Chan, C. K.: Aqueous secondary organic aerosol formation from the direct photosensitized oxidation of vanillin in the absence and presence of ammonium nitrate, *Atmos. Chem. Phys.*, 22, 273–293, <https://doi.org/10.5194/acp-22-273-2022>, 2022.
- Mazzoleni, L. R., Saranjampour, P., Dalbec, M. M., Samburova, V., Hallar, A. G., Zielinska, B., Lowenthal, D. H., and Kohl, S.: Identification of water-soluble organic carbon in non-urban aerosols using ultrahigh-resolution FT-ICR mass spectrometry: organic anions, *Environ. Chem.*, 9, 285–297, <https://doi.org/10.1071/EN11167>, 2012.
- Minero, C., Bono, F., Rubertelli, F., Pavino, D., Maurino, V., Pelizzetti, E., and Vione, D.: On the effect of pH in aromatic photonitration upon nitrate photolysis, *Chemosphere*, 66, 650–656, <https://doi.org/10.1016/j.chemosphere.2006.07.082>, 2007.
- Misovich, M. V., Hettiyadura, A. P. S., Jiang, W., Zhang, Q., and Laskin, A.: Molecular-level study of the photo-oxidation of aqueous-phase guaiacyl acetone in the presence of $^3\text{C}^*$: formation of brown carbon products, *ACS Earth Space Chem.*, 5, 1983–1996, <https://doi.org/10.1021/acsearthspacechem.1c00103>, 2021.
- Munger, J. W., Jacob, D. J., Waldman, J. M., and Hoffmann, M. R.: Fogwater chemistry in an urban atmosphere, *J. Geophys. Res. [Oceans]*, 88, 5109–5121, <https://doi.org/10.1029/JC088iC09p05109>, 1983.
- Nolte, C. G., Schauer, J. J., Cass, G. R., and Simoneit, B. R. T.: Highly polar organic compounds present in wood smoke and in the ambient atmosphere, *Environ. Sci. Technol.*, 35, 1912–1919, <https://doi.org/10.1021/es001420r>, 2001.
- Nozière, B., Dziedzic, P., and Córdova, A.: Products and kinetics of the liquid-phase reaction of glyoxal catalyzed by ammonium ions (NH_4^+), *J. Phys. Chem. A*, 113, 231–237, <https://doi.org/10.1021/jp8078293>, 2009.
- Nozière, B., Dziedzic, P., and Córdova, A.: Inorganic ammonium salts and carbonate salts are efficient catalysts for aldol condensation in atmospheric aerosols, *Phys. Chem. Chem. Phys.*, 12, 3864–3872, <https://doi.org/10.1039/B924443C>, 2010.
- Nozière, B., Fache, F., Maxut, A., Fenet, B., Baudouin, A., Fine, L., and Ferronato, C.: The hydrolysis of epoxides catalyzed by inorganic ammonium salts in water: kinetic evidence for hydrogen bond catalysis, *Phys. Chem. Chem. Phys.*, 20, 1583–1590, <https://doi.org/10.1039/C7CP06790A>, 2018.
- Pang, H., Zhang, Q., Lu, X., Li, K., Chen, H., Chen, J., Yang, X., Ma, Y., Ma, J., and Huang, C.: Nitrite-mediated photooxidation of vanillin in the atmospheric aqueous phase, *Environ. Sci. Technol.*, 53, 14253–14263, <https://doi.org/10.1021/acs.est.9b03649>, 2019.
- Powelson, M. H., Espelien, B. M., Hawkins, L. N., Galloway, M. M., and De Haan, D. O.: Brown carbon formation by aqueous-phase carbonyl compound reactions with amines and ammonium sulfate, *Environ. Sci. Technol.*, 48, 985–993, <https://doi.org/10.1021/es4038325>, 2014.
- Pye, H. O. T., Nenes, A., Alexander, B., Ault, A. P., Barth, M. C., Clegg, S. L., Collett, J. L. Jr., Fahey, K. M., Hennigan, C. J., Herrmann, H., Kanakidou, M., Kelly, J. T., Ku, I., McNeill, V. F., Riemer, N., Schaefer, T., Shi, G., Tilgner, A., Walker, J. T., Wang, T., Weber, R., Xing, J., Zaveri, R. A., and Zuend, A.: The acidity of atmospheric particles and clouds, *Atmos. Chem. Phys.*, 20, 4809–4888, <https://doi.org/10.5194/acp-20-4809-2020>, 2020.
- Raja, S., Raghunathan, R., Yu, X., Lee, T., Chen, J., Kommalapati, R. R., Murugesan, K., Shen, X., Qingzhong, Y., Valsaraj, K. T., and Collett, J. L. Jr.: Fog chemistry in the Texas-Louisiana Gulf Coast corridor, *Atmos. Environ.*, 42, 2048–2061, <https://doi.org/10.1016/j.atmosenv.2007.12.004>, 2008.



- 654 Rogge, W. F., Hildemann, L. M., Mazurek, M. A., and Cass, G. R.: Sources of fine organic aerosol. 9. Pine, oak, and
 655 synthetic log combustion in residential fireplaces, *Environ. Sci. Technol.*, **32**, 13–22, <https://doi.org/10.1021/es960930b>,
 656 1998.
- 657
- 658 Sagebiel, J. C., Seiber, J. N., and Woodrow, J. E.: Comparison of headspace and gas-stripping methods for determining the
 659 Henry's law constant (H) for organic compounds of low to intermediate H, *Chemosphere*, **25**, 1763–1768,
 660 [https://doi.org/10.1016/0045-6535\(92\)90017-L](https://doi.org/10.1016/0045-6535(92)90017-L), 1992.
- 661
- 662 Schauer, J. J., Kleeman, M. J., Cass, G. R., and Simoneit, B. R. T.: Measurement of emissions from air pollution sources. 3.
 663 C₁–C₂₉ organic compounds from fireplace combustion of wood, *Environ. Sci. Technol.*, **35**, 1716–1728,
 664 <https://doi.org/10.1021/es001331e>, 2001.
- 665
- 666 Shapiro, E. L., Szprengiel, J., Sareen, N., Jen, C. N., Giordano, M. R., and McNeill, V. F.: Light-absorbing secondary
 667 organic material formed by glyoxal in aqueous aerosol mimics, *Atmos. Chem. Phys.*, **9**, 2289–2300,
 668 <https://doi.org/10.5194/acp-9-2289-2009>, 2009.
- 669
- 670 Siegmann, K. and Sattler, K.: Formation mechanism for polycyclic aromatic hydrocarbons in methane flames, *J. Chem.*
 671 *Phys.*, **112**, 698–709, <https://doi.org/10.1063/1.480648>, 2000.
- 672
- 673 Simoneit, B. R. T.: Biomass burning — a review of organic tracers for smoke from incomplete combustion, *Appl.*
 674 *Geochem.*, **17**, 129–162, [https://doi.org/10.1016/S0883-2927\(01\)00061-0](https://doi.org/10.1016/S0883-2927(01)00061-0), 2002.
- 675
- 676 Simoneit, B. R. T., Rogge, W. F., Mazurek, M. A., Standley, L. J., Hildemann, L. M., and Cass, G. R.: Lignin pyrolysis
 677 products, lignans, and resin acids as specific tracers of plant classes in emissions from biomass combustion, *Environ. Sci.*
 678 *Technol.*, **27**, 2533–2541, <https://doi.org/10.1021/es00048a034>, 1993.
- 679
- 680 Simoneit, B. R. T., Schauer, J. J., Nolte, C. G., Oros, D. R., Elias, V. O., Fraser, M. P., Rogge, W. F., and Cass, G. R.:
 681 Levoglucosan, a tracer for cellulose in biomass burning and atmospheric particles, *Atmos. Environ.*, **33**, 173–182,
 682 [https://doi.org/10.1016/S1352-2310\(98\)00145-9](https://doi.org/10.1016/S1352-2310(98)00145-9), 1999.
- 683
- 684 Simpson, C. D., Paulsen, M., Dills, R. L., Liu, L.-J. S., and Kalman, D. A.: Determination of methoxyphenols in ambient
 685 atmospheric particulate matter: tracers for wood combustion, *Environ. Sci. Technol.*, **39**, 631–637,
 686 <https://doi.org/10.1021/es0486871>, 2005.
- 687
- 688 Slikboer, S., Grandy, L., Blair, S. L., Nizkorodov, S. A., Smith, R. W., and Al-Abadleh, H. A.: Formation of light absorbing
 689 soluble secondary organics and insoluble polymeric particles from the dark reaction of catechol and guaiacol with Fe(III),
 690 *Environ. Sci. Technol.*, **49**, 7793–7801, <https://doi.org/10.1021/acs.est.5b01032>, 2015.
- 691
- 692 Smith, D. F., Kleindienst, T. E., and McIver, C. D.: Primary product distributions from the reaction of OH with m-, p-xylene,
 693 1,2,4- and 1,3,5-trimethylbenzene, *J. Atmos. Chem.*, **34**, 339–364, <https://doi.org/10.1023/A:1006277328628>, 1999.
- 694
- 695 Smith, J. D., Sio, V., Yu, L., Zhang, Q., and Anastasio, C.: Secondary organic aerosol production from aqueous reactions of
 696 atmospheric phenols with an organic triplet excited state, *Environ. Sci. Technol.*, **48**, 1049–1057,
 697 <https://doi.org/10.1021/es4045715>, 2014.
- 698
- 699 Smith, J. D., Kinney, H., and Anastasio, C.: Aqueous benzene-diols react with an organic triplet excited state and hydroxyl
 700 radical to form secondary organic aerosol, *Phys. Chem. Chem. Phys.*, **17**, 10227–10237,
 701 <https://doi.org/10.1039/C4CP06095D>, 2015.
- 702



- Smith, J. D., Kinney, H., and Anastasio, C.: Phenolic carbonyls undergo rapid aqueous photodegradation to form low-volatility, light-absorbing products, *Atmos. Environ.*, 126, 36–44, <https://doi.org/10.1016/j.atmosenv.2015.11.035>, 2016.
- Sun, Y. L., Zhang, Q., Anastasio, C., and Sun, J.: Insights into secondary organic aerosol formed via aqueous-phase reactions of phenolic compounds based on high resolution mass spectrometry, *Atmos. Chem. Phys.*, 10, 4809–4822, <https://doi.org/10.5194/acp-10-4809-2010>, 2010.
- US EPA: Estimation Programs Interface Suite™ for Microsoft® Windows, v 4.1, United States Environmental Protection Agency, Washington, DC, USA, 2012.
- Wang, Y., Huang, D. D., Huang, W., Liu, B., Chen, Q., Huang, R., Gen, M., Mabato, B. R. G., Chan, C. K., Li, X., Hao, T., Tan, Y., Hoi, K. I., Mok, K. M., and Li, Y. J.: Enhanced nitrite production from the aqueous photolysis of nitrate in the presence of vanillic acid and implications for the roles of light-absorbing organics, *Environ. Sci. Technol.*, 55, 15694–15704, <https://doi.org/10.1021/acs.est.1c04642>, 2021.
- Wang, Y., Huang, W., Tian, L., Wang, Y., Li, F., Huang, D. D., Zhang, R., Mabato, B. R. G., Huang, R., Chen, Q., Ge, X., Du, L., Ma, Y. G., Gen, M., Hoi, K. I., Mok, K. M., Yu, J. Z., Chan, C. K., Li, X., and Li, Y. J.: Decay kinetics and absorption changes of methoxyphenols and nitrophenols during nitrate-mediated aqueous photochemical oxidation at 254 and 313 nm, *ACS Earth Space Chem.*, 6, 1115–1125, <https://doi.org/10.1021/acsearthspacechem.2c00021>, 2022.
- Yang, J., Au, W. C., Law, H., Leung, C. H., Lam, C. H., and Nah, T.: pH affects the aqueous-phase nitrate-mediated photooxidation of phenolic compounds: implications for brown carbon formation and evolution, *Environ. Sci.: Processes Impacts*, <https://doi.org/10.1039/D2EM00004K>, 2022.
- Yasmeen, F., Vermeylen, R., Szmigielski, R., Iinuma, Y., Böge, O., Herrmann, H., Maenhaut, W., and Claeys, M.: Terpenylic acid and related compounds: precursors for dimers in secondary organic aerosol from the ozonolysis of α and β -pinene, *Atmos. Chem. Phys.*, 10, 9383–9392, <https://doi.org/10.5194/acp-10-9383-2010>, 2010.
- Yaws, C. L.: Handbook of vapor pressure, volume 3: Organic compounds C8 to C28, Gulf Professional Publishing, 1994.
- Ye, Z., Qu, Z., Ma, S., Luo, S., Chen, Y., Chen, H., Chen, Y., Zhao, Z., Chen, M., and Ge, X.: A comprehensive investigation of aqueous-phase photochemical oxidation of 4-ethylphenol, *Sci. Total Environ.*, 685, 976–985, <https://doi.org/10.1016/j.scitotenv.2019.06.276>, 2019.
- Yu, G., Bayer, A. R., Galloway, M. M., Korshavn, K. J., Fry, C. G., and Keutsch, F. N.: Glyoxal in aqueous ammonium sulfate solutions: products, kinetics and hydration effects, *Environ. Sci. Technol.*, 45, 6336–6342, <https://doi.org/10.1021/es200989n>, 2011.
- Yu, L., Smith, J., Laskin, A., Anastasio, C., Laskin, J., and Zhang, Q.: Chemical characterization of SOA formed from aqueous-phase reactions of phenols with the triplet excited state of carbonyl and hydroxyl radical, *Atmos. Chem. Phys.*, 14, 13801–13816, <https://doi.org/10.5194/acp-14-13801-2014>, 2014.
- Yu, L., Smith, J., Laskin, A., George, K. M., Anastasio, C., Laskin, J., Dillner, A. M., and Zhang, Q.: Molecular transformations of phenolic SOA during photochemical aging in the aqueous phase: competition among oligomerization, functionalization, and fragmentation, *Atmos. Chem. Phys.*, 16, 4511–4527, <https://doi.org/10.5194/acp-16-4511-2016>.
- Zhang, Q. and Anastasio, C.: Conversion of fogwater and aerosol organic nitrogen to ammonium, nitrate, and NO_x during exposure to simulated sunlight and ozone, *Environ. Sci. Technol.*, 37, 3522–3530, <https://doi.org/10.1021/es034114x>, 2003.



752 Zhang, R., Gen, M., Huang, D. D., Li, Y. J., and Chan, C. K.: Enhanced sulfate production by nitrate photolysis in the
 753 presence of halide ions in atmospheric particles, *Environ. Sci. Technol.*, **54**, 3831–3839,
 754 <https://doi.org/10.1021/acs.est.9b06445>, 2020.

755
 756 Zhang, R., Gen, M., Fu, T-M., and Chan, C. K.: Production of formate via oxidation of glyoxal promoted by particulate
 757 nitrate photolysis, *Environ. Sci. Technol.*, **55**, 5711–5720, <https://doi.org/10.1021/acs.est.0c0819>, 2021.

758
 759 Zhang, R., Gen, M., Liang, Z., Li, Y. J., and Chan, C. K.: Photochemical reactions of glyoxal during particulate ammonium
 760 nitrate photolysis: Brown carbon formation, enhanced glyoxal decay, and organic phase formation, *Environ. Sci. Technol.*,
 761 **56**, 1605–1614, <https://doi.org/10.1021/acs.est.1c07211>, 2022.

762
 763 Zielinski, T., Bolzacchini, E., Cataldi, M., Ferrero, L., Graßl, S., Hansen, G., Mateos, D., Mazzola, M., Neuber, R., Pakszys,
 764 P., Posyniak, M., Ritter, C., Severi, M., Sobolewski, P., Traversi, R., and Velasco-Merino, C.: Study of chemical and optical
 765 properties of biomass burning aerosols during long-range transport events toward the Arctic in summer 2017, *Atmosphere*,
 766 **11**, 84, <https://doi.org/10.3390/atmos11010084>, 2020.

767
 768
 769
 770
 771
 772
 773
 774
 775
 776
 777
 778
 779
 780
 781
 782
 783
 784
 785
 786
 787
 788
 789
 790
 791



Table 1. Reaction conditions, initial GUA (and DMB or VL) decay rate constants, normalized abundance of products, average elemental ratios, and average carbon oxidation state ($\langle \text{OS}_C \rangle$) in each experiment. The reaction systems consisted of GUA (0.1 mM), DMB (0.01 mM), VL (0.01 mM), and AN (1 mM) under air-saturated conditions after 180 min of simulated sunlight irradiation. The UHPLC-HESI-Orbitrap-MS data were obtained in both positive (POS) and negative (NEG) ion modes.

Exp no.	Reaction conditions	Initial GUA (and DMB or VL) decay rate constants (min^{-1}) ^a	Normalized abundance of products ^b	Normalized abundance of N-containing compounds ^b	$\langle \text{O:C} \rangle^c$	$\langle \text{H:C} \rangle^c$	$\langle \text{N:C} \rangle^c$	$\langle \text{OS}_C \rangle^c$
1	GUA+DMB	GUA: $5.4 \times 10^{-2} \pm 3.0 \times 10^{-4}$ DMB: $6.7 \times 10^{-3} \pm 1.2 \times 10^{-4}$	376 ± 22	NA	POS: 0.34	0.91	NA	-0.22
					NEG: 0.40	0.94	NA	-0.15
2	GUA+DMB+AN	GUA: $4.8 \times 10^{-2} \pm 6.4 \times 10^{-4}$ DMB: $6.2 \times 10^{-3} \pm 6.5 \times 10^{-5}$	310 ± 4	114	POS: 0.28	0.94	0.12	-0.03
					NEG: 0.37	0.91	0.04	-0.05
3	GUA+VL	GUA: $1.4 \times 10^{-2} \pm 1.8 \times 10^{-4}$ VL: $3.3 \times 10^{-2} \pm 7.0 \times 10^{-4}$	94 ± 5	NA	POS: 0.41	0.91	NA	-0.10
					NEG: 0.40	0.94	NA	-0.14
3	GUA+VL+AN	GUA: $1.5 \times 10^{-2} \pm 1.6 \times 10^{-4}$ VL: $2.8 \times 10^{-2} \pm 4.9 \times 10^{-5}$	100 ± 2	8	POS: 0.31	1.02	0.02	-0.34
					NEG: 0.39	0.91	0.03	-0.02
5	GUA+AN	$8.1 \times 10^{-3} \pm 7.2 \times 10^{-5}$	23 ± 1	9	POS: 0.35	0.99	0.16	0.19
					NEG: 0.38	1.01	0.05	-0.08

^aThe data fitting was performed in the initial linear region. Each value is the average of results from triplicate experiments. Errors represent one standard deviation. ^bThe normalized product abundance was calculated using the data from UHPLC-HESI-Orbitrap-MS in the positive (POS) ion mode as the GUA signal from the negative (NEG) ion mode was weak, which may introduce significant uncertainties during normalization. The uncertainties were propagated from the changes in [GUA] measured using UHPLC-PDA and the MS signal intensities. The samples for experiments without AN (marked with NA) were not analyzed for N-containing compounds. ^cThe average elemental ratios ($\langle \text{O:C} \rangle$, $\langle \text{H:C} \rangle$, and $\langle \text{N:C} \rangle$) and $\langle \text{OS}_C \rangle$ were based on the UHPLC-HESI-Orbitrap-MS results and estimated using the signal-weighted method (Bateman et al., 2012). The $\langle \text{OS}_C \rangle$ of GUA, DMB, and VL are -0.57, -0.44, and -0.25, respectively.

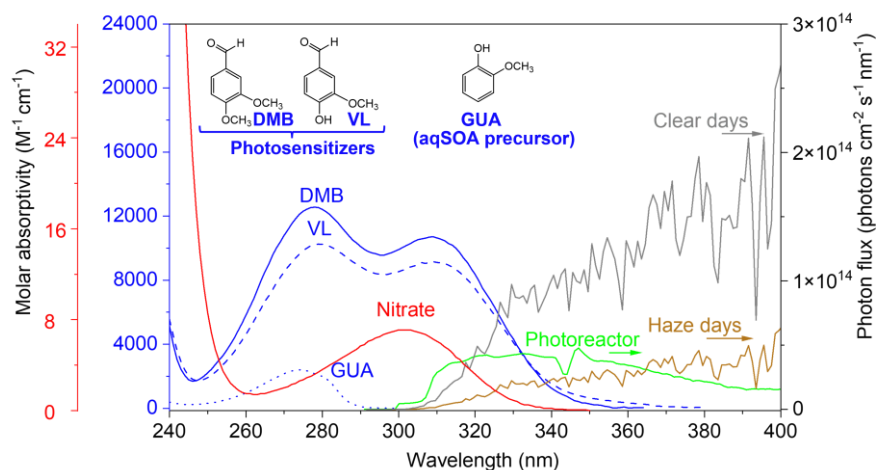


Figure 1. The base-10 molar absorptivities ($\text{M}^{-1} \text{cm}^{-1}$) of 3,4-dimethoxybenzaldehyde (DMB, blue solid line), vanillin (VL, blue dashed line), guaiacol (GUA, blue dotted line), and nitrate (red solid line). The green line is the photon flux in the aqueous photoreactor. The gray and brown lines are the photon fluxes on clear or haze days, respectively, in Beijing, China (Mabato et al., 2022). The top of the figure also shows the structures of DMB, VL, and GUA.

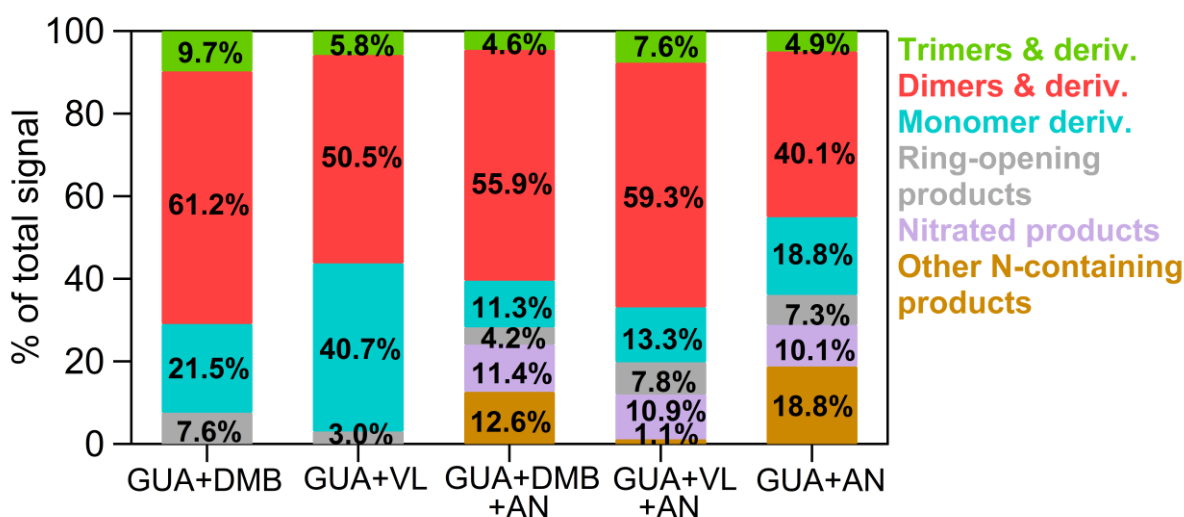


Figure 2. Signal-weighted distributions of aqSOA from GUA+DMB, GUA+VL, GUA+DMB+AN, GUA+VL+AN, and GUA+AN. These product distributions were calculated from combined UHPLC-HESI-Orbitrap-MS data obtained in positive (POS) and negative (NEG) ion modes. The values indicate the contribution of different product classifications to the total signals for each reaction condition.

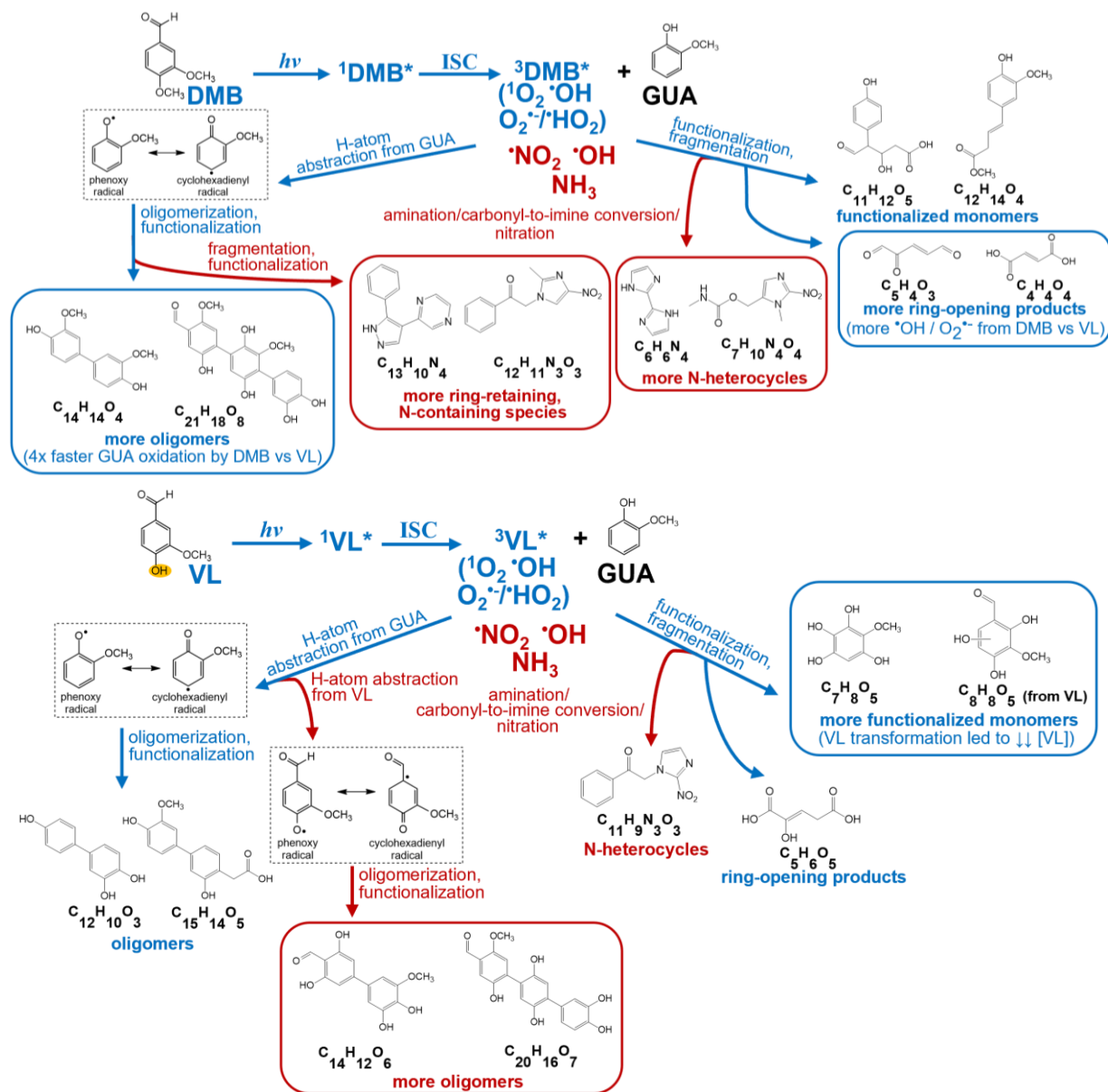


Figure 3. Summary of the main differences between photosensitized GUA oxidation by $^3\text{DMB}^*$ (top) and $^3\text{VL}^*$ (bottom) in the absence (blue labels and boxes) and presence (red labels and boxes) of ammonium nitrate at pH 4 under air-saturated conditions. Boxed structures indicate product classifications with notable differences. DMB and VL absorb light and are promoted to their singlet excited states ($^1\text{DMB}^*$ and $^1\text{VL}^*$), which then undergo intersystem crossing (ISC) to form $^3\text{DMB}^*$ and $^3\text{VL}^*$. Secondary oxidants ($^1\text{O}_2$, $\text{O}_2^{\cdot-}/\text{HO}_2$, OH) can be formed from $^3\text{DMB}^*$ and $^3\text{VL}^*$ upon reactions with O_2 and GUA (George et al., 2018; Chen et al., 2020; Misovich et al., 2021; Mabato et al., 2022). The structures shown are examples of the major products (Tables S1 to S4) for different product classifications.

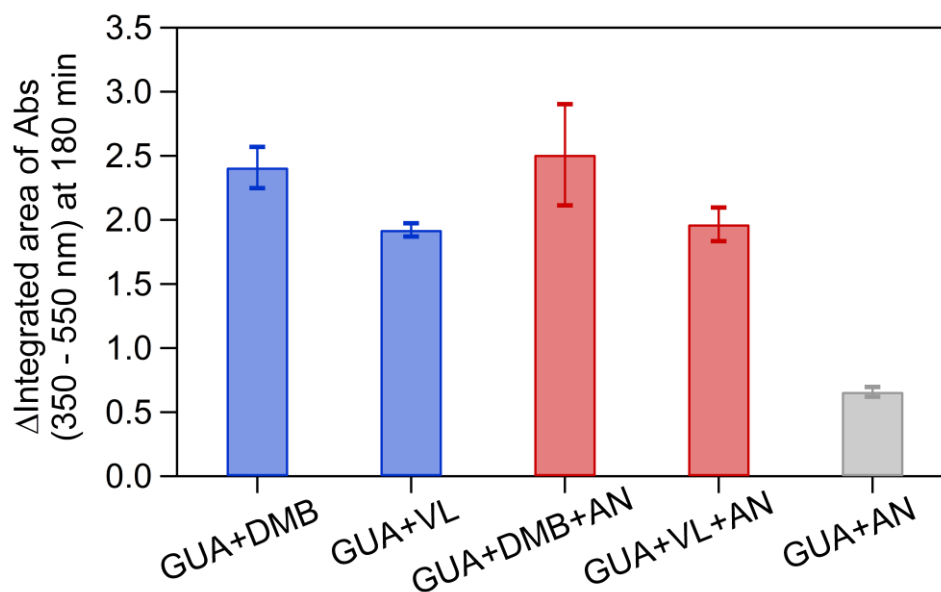


Figure 4. Increase in visible light absorption for aqSOA from GUA+DMB, GUA+VL, GUA+DMB+AN, and GUA+VL+AN. Error bars represent one standard deviation of triplicate experiments.